Received: 19 September 2022 | Revised: 7 December 2023 | Accepted: 13 January 2024

DOI: 10.1002/we.2899

RESEARCH ARTICLE

WILEY

Impact of yaw misalignment on turbine loads in the presence of wind farm blockage

Federico Bernardoni | **Mario A. Rotea** | **Stefano Leonardi**

UTD Wind, Department of Mechanical Engineering, University of Texas at Dallas, Richardson, Texas, USA

Correspondence
Stefano Leonardi, Department of Mechanical Engineering, University of Texas at Dallas, Richardson, TX 75080, USA.
Email: stefano.leonardi@utdallas.edu

Funding information
National Science Foundation, Grant/Award Numbers: 1916776, 1839733

Summary

Wake steering is very effective in optimizing the power production of an array of turbines aligned with the wind direction. However, the wind farm behaves as a porous obstacle for the incoming flow, inducing a secondary flow in the lateral direction and a reduction of the upstream wind speed. This is normally referred to as blockage effect. Little is known on how the blockage and the secondary flow influence the loads on the turbines when an intentional yaw misalignment is applied to steer the wake. In this work, we assess the variation of the loads on a virtual 4 by 4 array of turbines with intentional yaw misalignment under different levels of turbulence intensity. We estimate the upstream distance at which the incoming wind is influenced by the wind farm, and we determine the wind farm blockage effect on the loads. In presence of low turbulence intensity in the incoming flow, the application of yaw misalignment was found to induce a significant increase of damage equivalent load (DEL) mainly in the most downstream row of turbines. We also found that the sign (positive or negative) of the yaw misalignment affects differently the dynamic loads and the DEL on the turbines. Thus, it is important to consider both the power production and the blade fatigue loads to evaluate the benefits of intentional yaw misalignment control especially in conditions with low turbulence intensity upstream of the wind farm.

KEYWORDS
blade loads, wake steering, wind farm blockage, yaw control

1 | INTRODUCTION

The distribution of turbines in a wind farm may depend on multiple factors such as terrain topography, accessibility of the site, or cost minimization for the construction and maintenance. In most wind farms, the spacing among the wind turbines is dictated by the prevailing wind direction at the site. In particular, a smaller spacing is usually left in the direction perpendicular to the prevailing wind direction to maximize the wind energy extracted per unit of occupied land surface. However, the distribution of wind turbines in the wind farm may have significant consequences in terms of wake interaction (a low momentum region impinging on downstream turbines), modification of the local wind patterns, and maintenance on the turbines. In order to maximize the power production of a wind farm, the wake interaction among the wind turbines must be minimized. Several strategies have been proposed to reduce wake interaction and maximize power production[1,2]; a review is presented in Kheirabadi and Nagamune[3] and Andersson et al.[4] Among them, wake steering by yaw control, that is, the intentional application of yaw misalignment to upstream

turbines, has been shown to be a promising technique to increase the power production of arrays of aligned turbines[5] and of wind farms.[6–11] The power production of the yawed turbines decreases, but their wakes are steered away from the downstream turbines, which increase their power production. As a result, depending on the atmospheric conditions and the turbine spacing, the cumulative power production of the turbine array increases. The variability of the wind direction and the complexity of the wind farm challenge the practical application of yaw misalignment. It is, in fact, necessary to know in real time, while the wind is meandering, which turbines are in the wake of others (clusters of turbines). In our previous work,[12,13] we were able to identify the clusters in real time as the wind direction changes and reduce the complexity of the wind farm power optimization problem by optimizing each cluster instead of the entire farm.

The presence of the wind farm alters the local atmospheric boundary layer (ABL) not only downstream but also upstream by causing a decrease in wind speed and the development of secondary flows. This effect is usually referred to as wind farm blockage. To date, two main theories explain the wind farm blockage effect. The most common explanation is based on the hydrodynamic blockage of the wind farm. The array of turbines can be thought of as a large porous bluff body to the incoming atmospheric boundary layer flow. The pressure in the first row of turbines is higher than in the surrounding and causes the streams of air to divert towards the sides, in the direction of least resistance. Numerical[14–16] and wind tunnel[17,18] studies have been conducted to show the impact of the hydrodynamic blockage on the performance of wind turbines and wind farms. Nygaard et al[19] proposed a reduced-order model to predict the reduction of the incoming velocity, showing the importance of considering the blockage effect when estimating the performance of real wind farms. An alternative theory points to the excitation of atmospheric gravity waves by the wind farm as the main cause of the blockage effect. Gravity waves are mainly generated by the terrain topography.[20] Due to the interaction with the atmospheric boundary layer, the wind farm may also generate gravity waves[21] that, in turn, affect the power production due to the pressure feedback. Numerical simulations[22–24] have been performed to quantify the implications of wind farm induced gravity waves. Lanzilao and Meyers[25] showed that both gravity waves and hydrodynamic blockage contribute to the reduction of the velocity in front of the wind farm. However, gravity waves may also enhance the wake recovery due to a favorable pressure gradient established within the farm. Depending on the atmospheric conditions, the combination of the two theories further clarifies the physical source of the blockage effect.[26] Because of the blockage effect, Bleeg et al[27] and Schneemann et al[28] reported possible wind speed reductions of 2%–4% and 6% during field experiments, respectively. Additional field experiments, such as Debnath et al,[29] are still undergoing to collect full scale wind farm data to better undertsand blockage effects.

While several studies have focused on optimizing the wind farm power production, fewer studies have been conducted on the implications of the wind farm blockage on wake steering by yaw control. In Bernardoni et al,[30] we considered a 4 by 4 array of turbines with different spacing in the longitudinal and transversal directions. Depending on the wind direction, we found that the blockage effect of the wind farm plays an important role in determining the direction of the yaw misalignment (ψ) to be applied to the different turbines within the wind farm. In particular, when the turbine spacing in the direction perpendicular to the incoming wind is smaller, the blockage effect of the wind farm is larger affecting the yaw angle maximizing the power production. Meyers et al[31] also highlighted that the inclusion of the blockage effect can potentially change the optimal set points of clustered turbines.

In this study, we first quantify the blockage of the wind farm. Then, we use the previously optimized configuration of the wind farm to further analyze the effect on the turbines' loads under different incoming turbulence intensities. In particular, we assess how the yaw misalignment, optimized in presence of blockage effect, influences the damage equivalent load (DEL) of each turbine across the wind farm.

Section 2 of this paper presents the wind farm set up and the method employed in the numerical simulations; Section 3 quantifies the blockage of the wind farm and describes the implications of the blockage effect in the choice of the best yaw misalignment; Section 4 focuses on the fatigue loads of the turbines when yaw misalignment is applied to the wind farm; finally, Section 5 summarizes the findings of this work.

2 | NUMERICAL SET-UP

A virtual wind-farm composed of 16 NREL-5MW reference turbine,[32] arranged in four rows and four columns, is simulated with Large Eddy Simulations (LES). The turbines have a rotor diameter $D = 126\,\text{m}$, rated wind speed $U_{rated} = 11.4\,\text{m/s}$, and rated power $P_{rated} = 5\,\text{MW}$. As shown in Figure 1, the turbine spacing in the transversal direction (z direction) is $3D$, while in the longitudinal direction (x direction), the spacing is $5D$.

The spanwise spacing of the turbines affects the intensity of the blockage effect. The dependence on the turbine spacing goes beyond the scope of the present study. In this paper, we focus mostly on its effect on yaw control and optimization. The simulations have been performed with our in-house LES code UTD-WF. The filtered non-dimensional governing equations for incompressible flow are as follows:

$$\frac{\partial U_i}{\partial x_i} = 0 \tag{1a}$$

$$\frac{\partial U_i}{\partial t} + \frac{\partial U_i U_j}{\partial x_j} = -\frac{\partial P}{\partial x_i} + \frac{1}{Re}\frac{\partial^2 U_i}{\partial x_j \partial x_j} + \frac{\partial \tau_{ij}^{sgs}}{\partial x_j} + F_i \tag{1b}$$

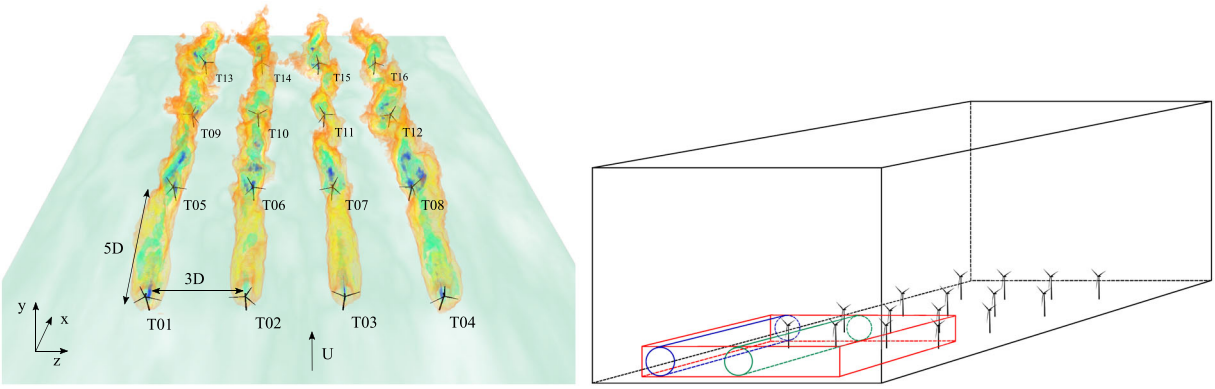

FIGURE 1 Layout of the virtual wind farm. Color contours identify the wakes that propagate downstream of the turbines. Regions colored in blue indicate low speed fluid, while regions in red represents higher speed fluid. The spacing between the turbines and their identification label is shown in the figure. On the right side of the figure, the computational domain is shown together with the control volumes used to evaluate the blockage effect: The red volume comprehends the entire area upstream of the wind farm, the blue cylinder considers only the region upstream of T01 rotor, and the green volume refers to a cylinder between two columns of turbines.

where U_i is the i^{th} component of the filtered velocity vector, P is the filtered modified pressure, $Re = U_{ref} D/\nu = 10^8$ is the Reynolds number, ν is the kinematic viscosity, τ_{ij}^{sgs} is the subgrid stress tensor, and F_i is the body force that accounts for the effects of the turbines on the aerodynamic field. Smagorinsky subgrid-scale model is used for modeling τ_{ij}^{sgs}. The index $i = (1,2,3)$ refers, respectively, to the streamwise (U), vertical (V), and spanwise (W) components of the velocity. The numerical discretization, discussed in Orlandi,[33] consists of a staggered central second-order finite-difference approximation in a cartesian coordinate system together with an hybrid low-storage third-order Runge-Kutta scheme to advance the equations in time. The energy equation is not included in the present set of simulations. The towers and nacelles are simulated using the immersed boundary method (IBM) implemented by Orlandi and Leonardi[34] and by Santoni et al.[35,36] The forces of the rotor acting on the flow are reproduced using the rotating actuator disk model.[37,38] The actual blades are replaced by the forces they apply to the flow. The local forces on each section of the blade are computed using the local relative velocity, angle of attack, and airfoil look-up tables. These forces are spread in the disk area with a Gaussian kernel.[36,39] The spreading distribution depends on both the radial distance and the azimuthal distance from the instantaneous position of the blade. Hence, the forces are applied in the governing equation through the body force term (F_i in Equation (1)). While previous studies have shown the importance of considering the aeroelastic coupling between the incoming flow and the blade structure,[40] for the present study, we limit our analysis to the aerodynamic loads on the blades.

The disk rotates in time with an instantaneous angular speed, ω, determined through the angular momentum balance between the aerodynamic torque T_{aero} and the generator torque M_{gen}:

$$I\dot{\omega} = T_{aero} - M_{gen} \tag{2}$$

where I is the rotor inertia. The generator torque is determined through a standard region II control law, according to which is proportional to the square of the generator speed[41,42]:

$$M_{gen} = k_{gen} \cdot \omega_{gen}^2 \tag{3}$$

where $\omega_{gen} = N_{gear} \cdot \omega$ is the high-speed shaft angular velocity, being N_{gear} the gear ratio ($N_{gear} = 97$). In equilibrium ($\dot{\omega} = 0$), the operating rotational speed is determined by the value of the torque gain k_{gen}. To achieve maximum efficiency, the torque gain is taken to be

$$k_{gen} = \frac{1}{N_{gear}^2} \frac{1}{2} \rho \pi R^5 \frac{C_P(\lambda_{opt})}{\lambda_{opt}^3} = 2.2 \text{Nm/rpm}^2 \tag{4}$$

where $\lambda_{opt} = 7.5$ is the optimal tip speed ratio for the NREL 5-MW reference turbine, R is the radius of the turbine, and C_p is the maximum power coefficient of the turbine. We regard the torque gain in Equation (4) as the ideal design value.

No-slip conditions are applied at the bottom boundary of the domain, on the nacelles and the towers of the turbines. Free-slip conditions are applied at the top boundary of the computational domain. Radiative boundary conditions[43] are given at the outlet of the domain. The computational box is $32D$, $10D$, and $19.2D$, respectively in the streamwise, vertical, and spanwise direction. A distance of $8D$ is left between the inlet and

the first row of turbines. A distance of 5.1D is left between each side of the wind farm and the computational domain to avoid that periodic boundary conditions at the later boundaries influence the flow within the wind farm.

The computational grid is uniform in the streamwise and spanwise direction with a grid spacing $\Delta x = \Delta z = 0.03D$. In the wall-normal direction, $n_2 = 192$ grid points were used; the first $m_2 = 80$ points (from $j = 1$ to 80) are uniformly spaced up to $y = 2D$. To limit the computational cost, above $y = 2D$, the grid is stretched with a hyperbolic tangent transformation:

$$y_j = \left(1 + \frac{\tanh(\beta(\xi_j - 0.5))}{\tanh(\beta/2)}\right) \cdot 8D + 2D \tag{5}$$

where j is the grid point, $\xi_j = \frac{j - m_2}{2(n_2 - m_2)}$ and $m_2 + 1 < j < n_2$. The value of $\beta \simeq 2.78$ is calculated to have continuity of Δy at the boundary between the uniform grid and the stretched grid. The grid is then smoothed to have continuity of $\partial \Delta y / \partial y$. Although the resolution is not sufficient to resolve accurately the boundary layer around the tower (as in most LES), the immersed boundary method provides impermeability, thus mimicking the blockage and the overall momentum loss. A similar grid resolution was adopted in a previous study[44] where we coupled our in-house code with the weather research and forecasting (WRF) model, thus solving with a good approximation the interaction between a real wind farm in North Texas and the meso-scale. Numerical results of power production and turbulent intensities at the turbines agreed well with SCADA data.

In order to reproduce the ABL, the mean velocity profile at the inlet is expressed by the following law:

$$\frac{\bar{U}}{U_{hub}} = \left(\frac{y}{y_{hub}}\right)^{\alpha} \tag{6}$$

where y is the vertical coordinate, y_{hub} is the hub height, and α is the shear exponent set to $\alpha = 0.05$. To study the influence of the turbulence intensity, two cases were considered. In the first, no inlet turbulence is imposed with a resulting turbulence intensity one diameter upstream of the wind farm of about 0.2%. In the second case, turbulent fluctuations obtained from a precursor simulation have been superimposed on the mean velocity profile in Equation (6) at the inlet. The precursor simulation is run in a computational box with periodic boundary conditions in both streamwise and spanwise direction, no-slip conditions at the bottom, and free-slip conditions at the top. Cubical roughness elements are placed on the ground (bottom of the computational domain) to enhance the generation of turbulence.[45] The superposition of the mean flow in Equation (6) and the turbulence from the precursor simulation results in a hub-height turbulence intensity of about 11% impinging the first turbine row of the wind farm. An additional simulation of the same domain without wind turbines was carried out in order to verify that the flow resulting from the superposition of the precursor simulation turbulence to the mean flow was completely developed. Neutral stability conditions without thermal stratification of the ABL are considered. While it was shown that stable conditions amplify the wind farm blockage effect,[16] the influence of the ABL stability on the wind farm performance goes beyond the scope of the present paper.

3 | BLOCKAGE EFFECT AND YAW CONTROL

In order to quantify the blockage effect of the wind farm on the incoming flow, we performed two sets of simulations with and without the wind turbines using the same boundary conditions; two cases, with low and high turbulence intensity at the inlet, were considered. To estimate the blockage effect, we compared the time averaged velocity fields obtained with and without the wind farm. It should be noted that the present study focuses on the estimation of the wind farm blockage due to only the hydrodynamic blockage as the gravity or thermal stratification are not considered in the simulations. As shown in the right pane of Figure 1, we computed the spatial average of the velocity field as function of the streamwise direction in 3 different regions of fluid:

1. a cylindrical region upstream of T01 (blue cylinder in Figure 1);
2. a cylindrical region between two columns of turbines upstream of the first row (green cylinder in Figure 1);
3. a rectangular region that covers the entire area upstream of the wind farm (red area in Figure 1).

Figure 2 shows the ratio between the averaged streamwise velocities with and without the wind farm in these three regions. In the region 1, that is, upstream of the turbine (blue line in Figure 2), the blockage effect of the wind farm sums up with the blockage effect of the single turbine. This produces the largest decreases in upstream streamwise velocity (about 3.2% one diameter upstream of the turbine). The velocity reduction in the second region (green line in Figure 2) indicates instead the blockage effect mostly caused by the presence of the wind farm, since there are no wind turbines located directly downstream of this region. Here, we notice a maximum decrease in wind speed of about 1.5% one diameter upstream of the wind farm. The velocity then increases again because the induction zones of T02 and T03 redirect the streams of fluid towards the center of the wind farm, thus increasing the local velocity. The red line in Figure 2 represents instead the average blockage effect of the wind

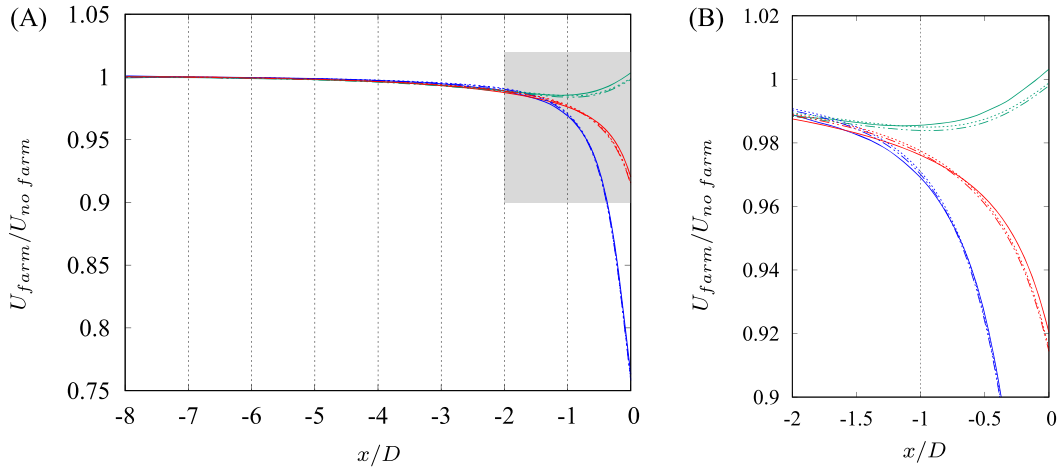

FIGURE 2 (A) Ratio between the averaged streamwise velocities obtained with and without wind farm; (B) enlarged view of the gray area of (A): ——— low turbulence at the inlet; – – – – low turbulence and larger computational domain; —··— high upstream turbulence. The colors of the lines refers to the 3D region used to average the velocity field (definition in Figure 1).

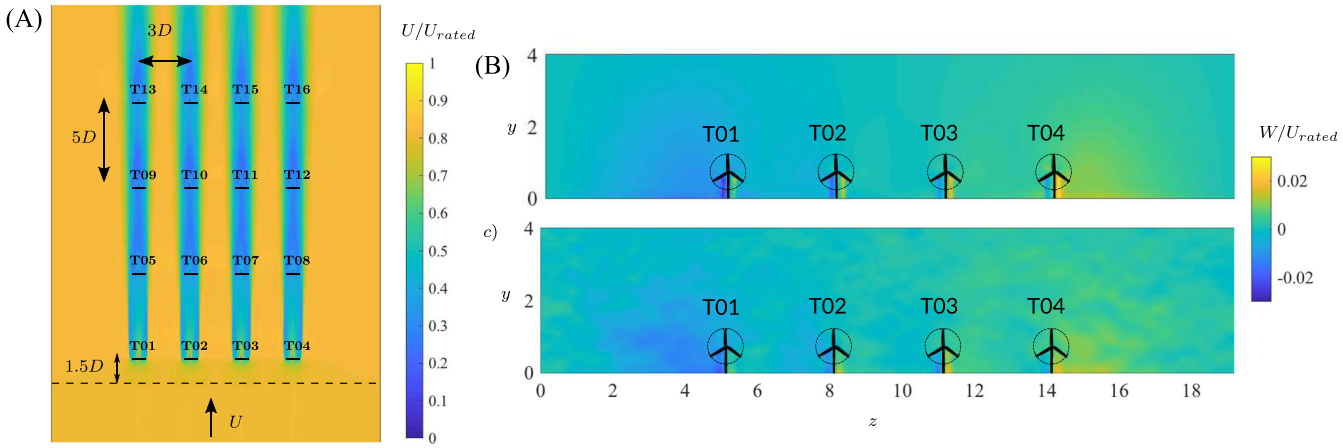

FIGURE 3 (A) Color contours of the time averaged velocity at hub height for the case with low inflow turbulent intensity. The rotor diameter of the turbines is denoted by *D*. (B–C) Color contours of the time-averaged spanwise velocity, *w*, at 1.5*D* in front of the first row of turbines without inlet turbulence (B) and with 11% turbulence intensity (C).

farm since it considers both the regions with and without turbines located downstream. We performed an additional simulation with a computational domain 2.5D wider on each side (therefore, with a total width of 24.2D) to evaluate possible blockage effects caused by the size of the computational domain. Figure 2 shows however a negligible effect of domain size on the average velocity variation in front of the wind farm. The wind farm blockage one diameter upstream is of about 2.5% consistently with the findings of previous studies.[16,28,46] Thus, since the wind turbine power production is proportional to the cube of the incoming velocity, the blockage of the wind farm can cause a reduction in power production of about 7% compared to estimations that use met-tower measurements performed in absence of the wind farm. Previous studies have shown that a more stable ABL increases the blockage effect of the wind farm.[16] In the present study, we instead simulated different level of turbulence intensity for a neutral ABL. However, Figure 2 shows that the presence of low or high turbulence upstream the wind farm does not significantly affect the blockage effect.

Figure 3 provides also an indication of the minimal distance upstream of the wind farm at which experimental measurements should be taken to estimate the blockage effect of an existing wind farm. In particular, under neutral stability atmospheric conditions, the upstream velocity should be measured at least 5.5*D* upstream of the first row of turbines to be within 0.1% of the incoming wind.

To assess the potential implications of the blockage effect on wind farm flow control, Figure 3B,C shows the spanwise component of the velocity 1.5*D* upstream of the first row of turbines, respectively, when uniform shear flow and turbulent flow are applied at the inlet. In both cases, a negative spanwise velocity (Westward) is observed in front of turbines T01 and T02, while a positive spanwise velocity (Eastward) is observed in front of T03 and T04. This is because the array of turbines can be thought of as a large porous bluff body to the incoming

atmospheric boundary layer flow. The stream of fluid is deflected towards the path of least resistance, that is, towards the sides of the wind farm. Hence, the secondary flow generated by the blockage effect changes the local wind direction with opposite sign at the two sides of the wind farm even if the prevailing wind direction is uniform upstream of the wind farm.

Wind farm power optimization through yaw control is based on deflecting the wakes of upstream turbines by imposing a controlled yaw misalignment angle. The power production of the turbine to which the yaw misalignment is applied decreases, but the downstream turbine faces a more energetic flow, thus increasing the cumulative power production of the array. However, the deflected wake of the yawed turbine tends to eventually realign to the local prevailing wind direction.[47–49] If the rotor is yawed consistently with the local wind direction induced by the blockage, the wake realigns further downstream, and thus, the power production gain of the trailing turbine is larger. Consequently, the yaw misalignment configuration that optimizes the wind farm power production has opposite direction at the two sides of the wind farm, as showed in Bernardoni et al.[30] For the considered wind direction, the optimal yaw misalignment corresponds to the following:

- $\psi = -20^\circ$ to the turbines in the West part of the wind farm (T01-T05-T09; T02-T06-T10);
- $\psi = +20^\circ$ to the turbines in the East part of the wind farm (T03-T07-T11; T04-T08-T12);
- no yaw misalignment to the most downstream turbines in each cluster (T13; T14; T15; T16).

This wind farm configuration was found to be the best performing among numerical simulations of the wind farm with yaw misalignment $\psi \in [-30^\circ, -20^\circ, -10^\circ, 10^\circ, 20^\circ, 30^\circ]$ applied to the upstream turbines. Figure 4A shows color contours of the mean velocity at the hub height of the optimized wind farm when no turbulence is applied at the inlet. The application of a finer resolution in the tested yaw angles may have provided a configuration with a slightly higher power production, as found for example by Munters and Meyers.[50] However, the emphasis here is not in the exact angle maximizing the power production but rather in assessing the influence of the blockage on the yaw misalignment. It should also be noted that the different wind directions imply different geometrical layout of the wind farm with respect to the incoming wind. Thus, depending on the layout, a wind farm can cause strong blockage effect for certain wind directions and negligible blockage for other wind directions.

4 | TURBINE LOADS

In order to assess the yaw misalignment influence on the turbines' loads, we first consider the case with low turbulence intensity in the incoming wind. Figure 4B,C reports a few cycles of the thrust force (T) at half of the blade span of T01 and T04 when the turbines are aligned with the local wind direction with and without yaw misalignment. In the baseline condition (Figure 4B), that is, without yaw misalignment ($\psi = 0^\circ$), both T01 and T04 experience a similar load cycle with T_{min} that corresponds to the tower shadow effect on the blade.[51,52] Indeed, in the lower region of the rotor disk in front of the turbine tower, the flow is deflected toward the sides of the tower determining a low velocity region in front of the tower and opposite spanwise velocity on the sides. Considering a counterclockwise rotation, when each blade passes in front of the tower, it encounters first a region with negative spanwise velocity followed by a region of slow flow due to the stagnation point on the tower and finally a region with positive spanwise velocity. This rapid change in the local spanwise velocity causes the sudden drop in the force experienced by the blade during each rotation cycle. As an example, the drop in the blade forces is showed at time 7 s in Figure 4B.

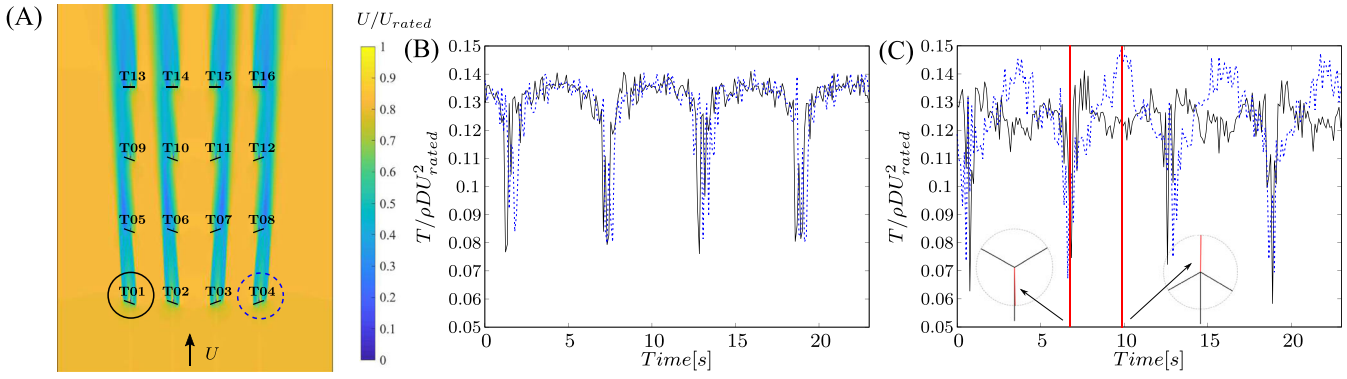

FIGURE 4 (A) Color contours of the time averaged velocity at hub height when optimal yaw misalignment is applied. (B, C) Thrust per unit length measured at half of the blade span of T01 (———) and T04 (– – – –) without yaw misalignment $\psi = 0$ (B) and with yaw misalignment of opposite direction ($\psi_{T01} = -20^\circ$) and T04 ($\psi_{T04} = +20^\circ$).

The difference between the maximum and minimum load that each blade experiences over each cycle, $\Delta T = T_{max} - T_{min}$, was used to characterize the magnitude of the load fluctuations. When yaw misalignment is applied (Figure 4C), T04 (dotted blue line) shows a much larger ΔT compared to T01 (solid black line). The minimum value T_{min} associated with the tower shadow (e.g., at $t = 7$ s in Figure 4C) decreases for both T01 and T04 compared to the baseline with $\psi = 0^\circ$ (Figure 4B). Independently of the direction of the yaw misalignment, the blade airfoil experiences a larger component of tailwind due to the tower shadow on the right side of the tower when $\psi \neq 0^\circ$ (with counterclockwise rotation of the blade).

The largest difference between T01 and T04 is instead observed when the blades pass in the higher part of the rotor disk (e.g., at $t = 10$ s in Figure 4C). The thrust force experienced by T04 is about 20% higher than that on T01 because of the opposite yaw misalignment angle necessary to optimize the power production in presence of the secondary motion induced by the wind farm blockage. Figure 5 shows a schematic of the relative velocities on the airfoil when the blade is on the top part of the rotor disk for different yaw angles. In this example, assuming a counterclockwise blade rotation, the relative velocity with respect to the airfoil (Ωr) is pointing rightward. The wind velocity (U) is kept constant in three cases, for example, $U = 0.8U_{rated}$. When the rotor plane is perpendicular to the wind direction (Figure 5A), the resulting relative velocity is given by the vector $\bar{u} = \bar{U} + \overline{\Omega r}$. The resulting magnitude of the relative velocity between the blade airfoil and the local flow is then given by $u = \sqrt{(\Omega r)^2 + U^2}$ while the angle of attack is $\alpha = \arctan(U/(\Omega r))$. Considering the airfoil at half of the blade span and the angular speed corresponding to the best tip speed ratio ($\lambda = 7.5$ for the NREL-5MW), the resulting relative velocity magnitude and angle of attack seen by the airfoil are, respectively, $u = 3.86U_{rated}$ and $\alpha = 15^\circ$. For sake of simplicity, the calculation is done under the hypothesis of 0° twist angle of the blade but the same rationale holds even for non-zero twist angles. When yaw misalignment ψ is applied, the component of the wind velocity U aligned with the rotor plane is $U\sin(\psi)$ while the component perpendicular to the rotor plane is $U\cos(\psi)$. Therefore, the velocity magnitude u and the angle of attack α of the flow in respect to the airfoil are given, respectively, by

$$u = \sqrt{(\Omega r + U\sin(\psi))^2 + (U\cos\psi)^2} \tag{7a}$$

$$\alpha = \arctan\left(\frac{U\cos(\psi)}{(\Omega r + \sin(\psi))}\right) \tag{7b}$$

As a consequence, the velocity magnitude and the angle of attack depend on the sign of the yaw misalignment angle ψ. In particular,

- if $\psi < 0$ (Figure 5B), the velocity magnitude decreases while the angle of attack increases (in the above example of the NREL-5MW $u = 3.52U_{rated}$ and $\alpha = 15.5^\circ$ for $\psi = -20^\circ$);
- if $\psi > 0$ (Figure 5C), the velocity magnitude increases, and the angle of attack decreases (in the example $u = 4.18U_{rated}$ and $\alpha = 13.0^\circ$ for $\psi = +20^\circ$).

The lift (L) of an airfoil is given by

$$L = \frac{1}{2}\rho c u^2 C_{L\alpha}\alpha \tag{8}$$

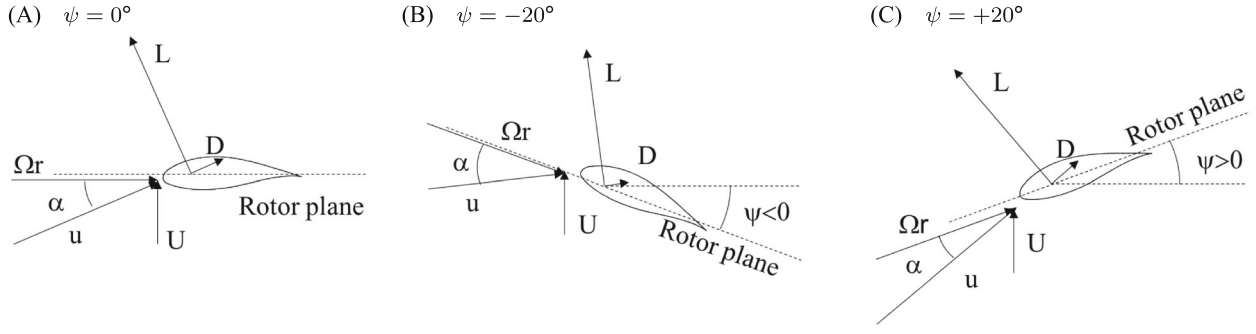

FIGURE 5 Schematics of the airfoil when the blade is positioned upwards of the rotor disk with different yaw misalignment: (A) no yaw misalignment ($\psi = 0^\circ$), (B) negative yaw misalignment ($\psi < 0^\circ$), and (C) positive yaw misalignment ($\psi > 0^\circ$). The force vectors are not to scale for sake of clarity. L and D identify, respectively, the lift and drag, Ω is the angular speed of the rotor, r is the radius of the blade section, U represents the wind velocity while u represents the sum of the wind velocity and relative speed due to the blade rotation.

where ρ is the air density, c is the airfoil chord, and $C_{L\alpha}$ is the slope of the $C_L - \alpha$ curve of the airfoil. Since the airfoil lift is the main force that is responsible for the turbine thrust force and torque, we can compare the blade loads under opposite yaw misalignment computing the ratio of the lift on the airfoil with $\psi = +20^\circ$ and $\psi = -20^\circ$:

$$\frac{L_{(\psi=+20^\circ)}}{L_{(\psi=-20^\circ)}} = \frac{u^2_{(\psi=+20^\circ)}\alpha_{(\psi=+20^\circ)}}{u^2_{(\psi=-20^\circ)}\alpha_{(\psi=-20^\circ)}} \tag{9}$$

Using the example of the NREL-5MW turbine above, $L_{(\psi=+20^\circ)}/L_{(\psi=-20^\circ)} = 1.184$. This means that in the top part of the rotor, the blade loads for positive yaw misalignment are about 18.4% higher than in the case of negative yaw misalignment. This simplified analytical analysis agrees very well with the results obtained from the numerical simulation where a difference of about 20% in the resultant aerodynamic force is observed on the top part of the rotor between the blades of T01 and T04 that have, respectively, $\psi_{T01} = -20^\circ$ and $\psi_{T04} = +20^\circ$ (see, for instance, at time $t \simeq 10$ s in Figure 4C).

This is further corroborated by the power spectral density (*PSD*) of the resultant aerodynamic force taken at half of the blade span shown in Figure 6 for T01 and T04. Both turbines have peaks for frequencies that correspond to the multipliers of the rotor angular speed frequency (for $\psi = 0^\circ$, $1P = 1.9U_{rated}/D$). For the baseline case, that is, $\psi = 0^\circ$ (black line), the PSD peaks associated with 1*P* of T01 and T04 have the same magnitude. On the contrary, when the two turbines have opposite yaw angles, the 1*P* peak relative to T01 is smaller than the baseline while that relative to T04 is higher. This indicates that positive yaw misalignment induces higher load fluctuations.

In order to quantify how the observed variation of turbine loads under different yaw misalignment affects the fatigue life of the blade, the Damage Equivalent Load (DEL) associated to the thrust force at half of the blade span is computed. Using the thrust load signal in time, the load cycles are computed using the rainflow counting method.[53] Then, following Palgrem-Miner's rule,[54] the DEL is evaluated as

$$DEL = \left(\frac{\sum_{i=1}^{n} \Delta T_i^m \cdot N_i}{N_{ref}}\right)^{1/m} \tag{10}$$

where m is the inverse of the material Wöhler slope ($m = 10$ for fiber glass), N_{ref} is the reference number of cycles taken equal to 1 here, ΔT_i is the load range for the i^{th} bin, and N_i is the total number of occurrence within the i^{th} bin.

Due to the wake interaction, the DEL across the wind farm is not uniform. We can consider the average DEL of the upstream row of turbines (T01, T02, T03, and T04) with $\psi = 0^\circ$ as representative of the DEL that an isolated turbine must withstand in absence of upstream turbulence (hereafter $DEL_{Bas-Lam}$). Figure 7A shows in red the ratio between the DEL of each turbine and the $DEL_{Bas-Lam}$ when each turbine is aligned with the local wind direction. The second row of turbines (T05, T06, T07, and T08) is characterized by a DEL reduction of about 40% compared to the baseline. This is because in the absence of upstream turbulence, the wake of the upstream row of turbines is not recovered before impinging on the downstream turbines. Therefore, the magnitude of the load fluctuations is limited by the low speed and strong coherence of the upstream turbine wake. The mean velocity color contours in the background of Figure 7A show much wider wakes impinging on the last row of turbines (T13, T14, T15, and T16) compared to the wakes in the second row. Moving downstream in the wind farm, the interaction of the upstream wakes with the other turbines increases the turbulent mixing and the energy entrainment into the wakes from the surrounding flow. Turbulence in the wakes of downstream turbines is therefore affected by the upstream wakes by an increase in mixing and a reduction in the size of the coherent turbulent structures. Therefore, the DEL of the last row of turbines is much larger than that on the second row of turbines due to larger fluctuations in the

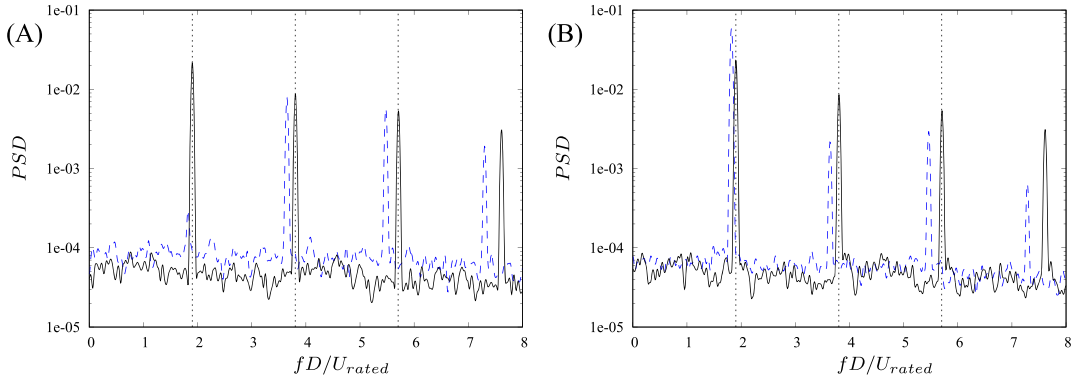

FIGURE 6 Power spectral density of the thrust load at half of the blade span for turbine T01 (A) and T04 (B). – – – – $\psi = 0^\circ$; ——— $\psi = -20^\circ$ for T01 (A) and $\psi = +20^\circ$ for T04 (B). Vertical dotted lines highlight the multipliers of the blade rotational frequency.

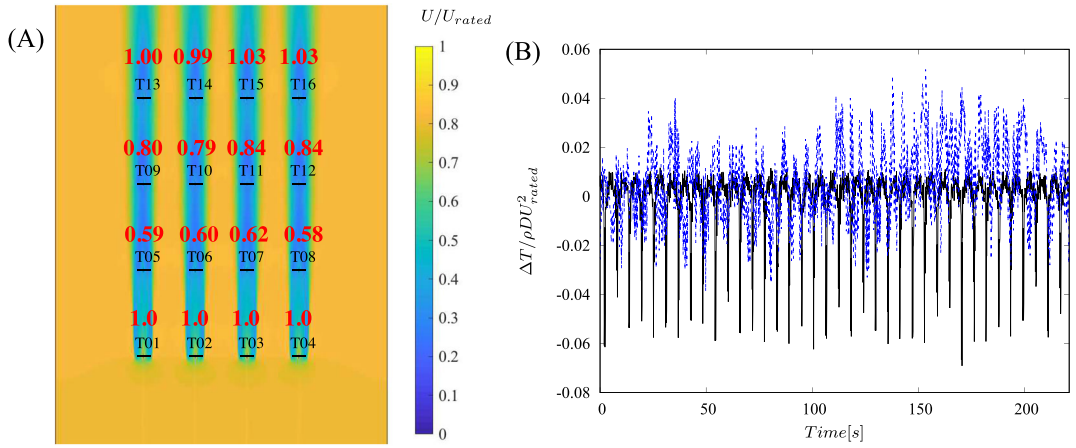

FIGURE 7 (A) Ratio of each turbine DEL and $DEL_{Bas-Lam}$; color contours of the mean velocity in the back-ground. (B) Thrust load fluctuations at half of the blade span of T03 (– – – –) and T15 (———) with $\psi = 0^\circ$ within the wind farm.

TABLE 1 Variation of DEL due to the application of yaw misalignment.

		$\frac{DEL_{YawOFF}}{DEL_{Bas-Lam}}$	$\frac{DEL_{YawON}}{DEL_{Bas-Lam}}$
Row 1	T01	1.00	1.04
	T02	1.00	1.04
	T03	1.00	1.14
	T04	1.00	1.11
Row 2	T05	0.59	0.94
	T06	0.60	0.95
	T07	0.62	1.12
	T08	0.58	1.13
Row 3	T09	0.80	1.18
	T10	0.79	1.18
	T11	0.84	1.31
	T12	0.84	1.32
Row 4	T13	1.00	1.51
	T14	0.99	1.52
	T15	1.03	1.50
	T16	1.03	1.58

Note: $DEL_{Bas-Lam}$ is the average DEL of the upstream row of turbines with no yaw misalignment.

incoming velocity. Despite the lower momentum, the last row of turbines has about the same DEL level of the most upstream row because of the loss of wake coherence and the associated higher turbulence. Figure 7B shows the fluctuations of the thrust load at half of the blade span for T03 and T15, a turbine in the most upstream and most downstream rows respectively. Only 200 s of the 30 min simulated are shown for clarity. The value of DEL of the two turbines is about the same but the source of the load fluctuations is different. The load fluctuations for T03, that is, the upstream turbine, are mostly due to the tower shadow effect leading to a very regular path in the fluctuations over time. On the other hand, the turbulent flow impinging on T15, that is in waked conditions, causes more chaotic fluctuations at different frequency and magnitude.

Table 1 reports the comparison of the DEL for all turbines in the wind farm when $\psi = 0^\circ$ and when they are at optimal yaw angle (see Section 3). As expected from the previous analysis, the turbines with negative yaw angle (T01, T02, T05, T06, T07, T09, and T10) exhibit a smaller variation in DEL compared to those with a positive yaw (T03, T04, T07, T08, T11, T12, T15, and T16). The turbines in the second row experience the largest variation in DEL (from about 0.60 to 1.13$DEL_{Bas-Lam}$). However, even in the yawed configuration, the increased DEL of the second row of turbines is about 13% compared to the baseline reference.

Due to the loss of coherence in the turbine wakes, the last row of turbines experiences the same DEL of the first row of turbines, even if the power production is much reduced due to the wake interaction. When yaw misalignment is applied to the upstream turbines, the DEL of T16 is the largest, about of +58% above the baseline. This represents a potential hazardous situation for the structural integrity of the blades, with a possible reduction in the fatigue life.

It should also be noted that despite the difference in the blade load between turbines with positive and negative ψ, the power production of the cluster T01-T05-T09-T13 is smaller than the power production of the cluster T04-T08-T12-T16 of only about 0.6% when yaw misalignment is applied. This is because the power production is mostly influenced by the flow averaged over the rotor area, while the load cycle is mostly affected by the local flow conditions that the blades experiences over the rotation. The direct implication on the wind farm operations is that, in the presence of low turbulence intensity, it may be convenient to reduce the power gain due to yaw misalignment to reduce the fatigue damage on the blades by applying positive yaw misalignment even to the clusters that would benefit from having $\psi < 0$.

The low turbulence intensity in front of the wind farm however may not be representative of realistic atmospheric conditions. Additionally, due to the computational limitation for the grid resolution, the Smagorinsky sub-grid model may lead to an artificial stabilization of the wakes. In the next section, we analyze instead a more realistic condition with a higher turbulence intensity level.

4.1 | Effect of incoming turbulence

In order to test how the wind turbine loads change in the presence of upstream turbulence, a new set of simulations was carried out imposing at the inlet a turbulent flow obtained from a precursor simulation (as described in Section 2). The resulting turbulence intensity averaged over the rotor disk is 9%, 11%, 11%, and 12% one diameter upstream of T01, T02, T03, and T04, respectively. In realistic conditions, turbulence intensity may vary across the wind farm with a not uniform distribution across the most upstream turbines. In fact, the incoming flow presents large-scale coherent structures that meander over the wind farm and cause slightly different DELs on the turbines in the first row (Table 2). In the present study, we simulated 30 min of real time during which the wind direction is assumed to be constant. Depending on the particular site and atmospheric conditions, the wind direction may remain constant for a longer time, and in that case, the DEL distribution would be more uniform. Since we are analyzing how the DEL varies with and without yaw misalignment on the different rows of the wind farm, rather than on the single turbine, the variability within one row does not affect our discussion or conclusions.

For the case with turbulent inflow, the baseline DEL ($DEL_{Bas-Turb}$) is taken as the average DEL of the first row of turbines. Due to the turbulent upstream conditions, larger fluctuations in the incoming velocity are experienced by the upstream row of turbines. As a consequence, the

TABLE 2 Variation of DEL due to the application of yaw misalignment in the presence of turbulence.

		$\frac{DEL_{YawOFF}}{DEL_{Bas-Turb}}$	$\frac{DEL_{YawON}}{DEL_{Bas-Turb}}$
Row 1	T01	0.95	0.97
	T02	0.95	0.98
	T03	0.94	0.99
	T04	1.14	1.17
Row 2	T05	0.67	0.74
	T06	0.65	0.81
	T07	0.61	0.82
	T08	0.95	0.90
Row 3	T09	0.72	0.84
	T10	0.77	0.90
	T11	0.77	0.91
	T12	1.14	0.99
Row 4	T13	0.82	1.01
	T14	0.77	0.98
	T15	0.89	1.01
	T16	1.03	1.12

Note: $DEL_{Bas-Turb}$ is the average DEL of the upstream row of turbines with no yaw misalignment and turbulent inlet is considered.

$DEL_{Bas-Turb}$ is about 1.9 times higher than $DEL_{Bas-Lam}$ used in the previous analysis. Even if with higher variability among the turbines in the same row due to incoming turbulence, the DEL across the wind farm varies similarly to the case with laminar inlet (Table 1). When $\psi = 0^\circ$, the DEL is minimum in the second row of turbines, and then, it increases moving downstream in the wind farm. When the turbines are yawed, the DEL of almost every turbine in the wind farm increases as expected with a trend similar to that observed for the laminar case (Table 2). However, the maximum DEL reached in the most downstream row of turbines is within 10% of the baseline value $DEL_{Bas-Turb}$. Therefore, the fatigue loads on yawed turbines are not significantly higher than those on an isolated turbine under turbulent incoming flow. This is in contrast with the case without incoming turbulence, where the DEL in the last row of turbines increases up to 58%.

To understand the reason of this major difference, we further analyze turbine T15 by plotting the PSD of the normal force at half span of the blade for both low and high turbulence intensity (Figure 8). The black solid line is relative to the case where all turbines have $\psi = 0^\circ$ while the blue dashed line represents the case with yawed turbines (yaw angles were given in Section 3). In both cases, T15 is not yawed, because it is in the last row of the farm. However, when the upstream turbines are yawed, the rotor of T15 is only partially in wake conditions (the wake of the upstream turbines partially reaches the rotor disk of T15). All spectra show a peak at very low frequencies between $0.04D/U_{rated}$ and $0.2D/U_{rated}$. For laminar inflow, (Figure 8A), the peak is related to turbulence developed within the wind farm as a consequence of the interaction between the wake and the turbines. On the other hand, when the incoming wind is turbulent (Figure 8B), the peak in the PSD is larger and due to large coherent turbulent structures in the incoming flow. The energy associated with the low frequency peak (slow load fluctuations) is not significantly affected by the application of the yaw misalignment in the wind farm (comparison of the black solid and blue dashed line in Figure 8). Major differences instead are observed on the peak relative to the turbine rotation $P1 = fD/U_{rated} = 1$.

When yaw misalignment is applied to the upstream turbines in the wind farm, the wake is partially steered away from the rotor of T15. The momentum of the flow on part of the rotor increases and so does the torque. Therefore, the rotational speed and the power production of T15 increase compared to the configuration where all the turbines in the wind farm are aligned with the wind direction. This increase in the rotational speed of the rotor is visible in the load spectra from the shift of the frequency of the 1P peak (i.e., the frequency associated with the turbine rotational speed). When the turbulence intensity upstream of the wind farm is low (Figure 8A), the frequency of the 1P peak in the spectra increases of about 38% while with high turbulence intensity upstream of the wind farm (Figure 8B), the frequency of the 1P peak increases of only about 11%. For low turbulence intensity upstream of the wind farm (Figure 8A), the configuration of the wind farm with yaw misalignment (dashed blue line) has the maximum value of the 1P peak about one order of magnitude higher than the condition where each turbine is aligned with the local wind direction. In the other case with higher turbulence intensity upstream of the wind farm (Figure 8B), the application of yaw misalignment increases the maximum value of the 1P peak of only about two times compared to the case when all turbines are aligned with the local wind direction. Hence, with respect to the baseline, the DEL of T15 increases because of the increase in the PSD of the 1P peak and because of the increase in its frequency. Since the DEL is proportional to the number of cycles N_i (see Equation (10)), a higher frequency of the loads implies a higher fatigue load given a fixed amount of operational time. When the incoming flow is turbulent, the PSD of the 1P peak and its frequency increase less than the correspondent laminar case. Ambient turbulence has a dual effect. On one side, it increases the blade load fluctuations due to the velocity variations upstream of the wind farm. On the other side, it enhances mixing and the wake recovery, thus alleviating the downstream turbines from the load fluctuations associated with large scale velocity gradients (as a laminar wind turbine wake which partially impinges on a turbine). Turbulence increases high frequency fluctuations at small scales and reduces those at low frequency and large scale.

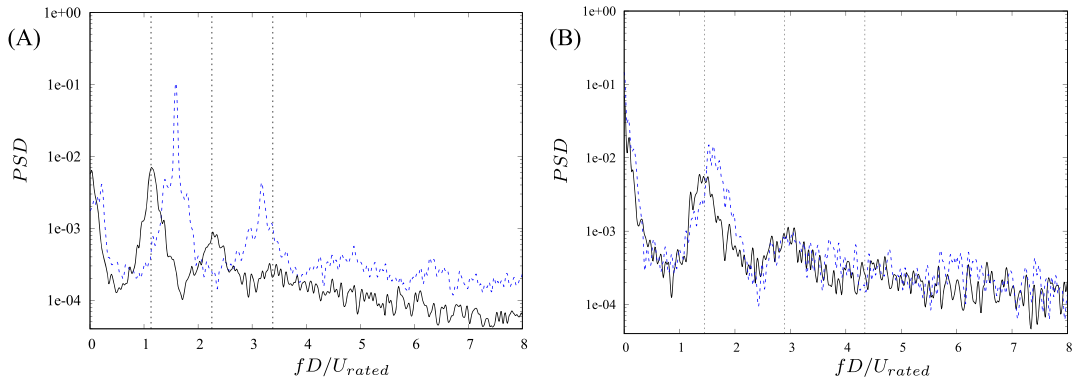

FIGURE 8 Power spectral density of the thrust load at half of the blade span for turbine T15 with low (A) and with high (B) turbulence intensity upstream of the wind farm: ——— $\psi = 0^\circ$ within the wind farm; – – – – yawed turbines (as in Section 3). Vertical dotted lines highlight the multipliers of the blade rotational frequency for the case without imposed yaw misalignment.

From Tables 1 and 2 and from the comparison of Figure 8A,B, we can summarize the following:

- in the presence of low turbulence intensity upstream of the wind farm, the application of yaw misalignment to increase the power production of the wind farm may result in a significant increase on the fatigue loads on the most downstream row of turbines. Especially in the case of wind farms with high density and numerous rows of turbines, the application of yaw misalignment should take into account both the power production and the fatigue loads on the blades.
- when higher turbulence intensity is present upstream of the wind farm, the DEL in the most downstream row of turbines increase up to about 10% compared to the most upstream row of turbines, indicating that the turbines need to withstand only a slightly higher DEL that what they normally experience for atmospheric turbulence.

Present results show the importance of the interaction between the blockage effect, turbulence intensity and yaw misalignment. However, more studies are needed to extrapolate the results to deep arrays of wind turbines. It should be also noted that the present analysis is carried out considering a specific wind condition while the turbine DEL is determined by considering the multitude of wind conditions that the wind farm experience over the year. Additionally, the density of the wind turbines, especially in the direction orthogonal to the prevalent wind direction, may play a significant role that is not investigated in the present paper.

5 | CONCLUSIONS

A wind farm constitutes an obstacle for the incoming flow that can create a high pressure region in front of the most upstream wind turbines. This phenomenon, known as wind farm blockage effect, can reduce the velocity in front of the wind farm about 2.5% with a potential loss in power production of 7% compared to analysis performed with met–tower measurements far from the wind farm. Under neutrally stable atmospheric conditions, we found that measurements of wind velocity unaffected by the presence of the wind farm should be taken at least 5.5D upstream of the first row of turbines to have an error smaller than 0.1% on the intensity of the incoming wind (U_∞). In addition to reducing the wind speed upstream of the wind farm, the blockage effect also redirects the flow stream on the sides and above the wind farm. The spanwise component of the velocity caused by the wind farm blockage have direct impact on the wind farm yaw control, since the direction of the wake steering should be chosen accordingly to the direction of the local spanwise velocity caused by the blockage. The impact of blockage effect on wake steering should be however carefully evaluated based on the layout of the wind farm since it is influenced by the spanwise spacing of the turbines as shown in Bernardoni et al.[30]

We found that, in the presence of low turbulence intensity, the direction of the yaw misalignment affects the fatigue loads on the blades. We considered the loads on the most upstream turbines as baseline. In the presence of low turbulence intensity upstream of the wind farm, the application of yaw misalignment may increase the DEL of the most downstream row of turbines up to about 50% compared to the baseline loads. On the other hand, when higher turbulence intensity is present upstream of the wind farm, the fatigue loads on the most downstream row of turbines do not increase much over the level of the most upstream turbine row of the wind farm. The load fluctuations the turbines encounter with yaw misalignment are not significantly higher that those due to the incoming turbulence.

While reduced order models have been developed to estimate power production variation associated with yaw misalignment, the dynamic nature of the fatigue loads makes more challenging the estimation of the DEL. This study provides evidence of the need to couple the power production with the fatigue loads when yaw misalignment is imposed in the presence of low turbulence intensity. The findings of this paper also open the possibility to tailor future wind farms to the local prevailing flow conditions. Indeed, maximizing the energy extracted from the wind in the presence of blockage effects may require optimized operations (e.g., modification of control parameters to accommodate the wind farm blockage). In addition, the choice of the yaw misalignment direction based on the blade rotational direction can reduce the variation of DEL. Thus, for wind farms located in sites with a prevailing wind direction, it may be convenient to have turbines with opposite rotational direction at the different sides of the wind farm.

The levelized cost of energy considers both the revenues coming from the farm power production and the costs associated with the turbine maintenance. Therefore, both the annual energy production increase and the turbine DEL variation should be considered by a control algorithm that aims to reduce the costs of wind energy.

ACKNOWLEDGMENTS

This material is based upon work supported by the National Science Foundation under Award Number 1916776, Phase II IUCRC at UT Dallas: Center for Wind Energy Science, Technology and Research (WindSTAR), The WindSTAR IUCRC Members and NSF Award Number 1839733. Any opinions, findings and conclusions or recommendations expressed in this material are those of the authors and do not necessarily reflect the views of the National Science Foundation or WindSTAR members. TACC is acnkowledged for providing computational time.

PEER REVIEW

The peer review history for this article is available at https://www.webofscience.com/api/gateway/wos/peer-review/10.1002/we.2899.

DATA AVAILABILITY STATEMENT

The data that support the findings of this study are available from the corresponding author upon reasonable request.

ORCID

Mario A. Rotea https://orcid.org/0000-0002-4239-0591
Stefano Leonardi https://orcid.org/0000-0002-4570-2255

REFERENCES

1. Meyers J, Meneveau C. Optimal turbine spacing in fully developed wind farm boundary layers. *Wind Energy*. 2012;15(2):305-317.
2. Padrón AS, Thomas J, Stanley APJ, Alonso JJ, Ning A. Polynomial chaos to efficiently compute the annual energy production in wind farm layout optimization. *Wind Energy Sci*. 2019;4(2):211-231.
3. Kheirabadi AC, Nagamune R. A quantitative review of wind farm control with the objective of wind farm power maximization. *J Wind Eng Ind Aerodyn*. 2019;192:45-73.
4. Andersson LE, Anaya-Lara O, Tande JO, Merz KO, Imsland L. Wind farm control—part I: a review on control system concepts and structures. *IET Renew Power Gener*. 2021;15(10):2085-2108.
5. Ciri U, Rotea MA, Leonardi S. Effect of the turbine scale on yaw control. *Wind Energy*. 2018;21(12):1395-1405.
6. Doekemeijer BM, van der Hoek D, van Wingerden J-W. Closed-loop model-based wind farm control using FLORIS under time-varying inflow conditions. *Renew Energy*. 2020;156:719-730.
7. Ciri U, Rotea M, Leonardi S. Increasing wind farm efficiency by yaw control: beyond ideal studies towards a realistic assessment. In: Torque 2020: The Science of Making Torque from Wind; 2020.
8. Fleming P, Sinner M, Young T, Lannic M, King J, Simley E, Doekemeijer B. Experimental results of wake steering using fixed angles. *Wind Energy Sci Disc*. 2021;2021:1-18.
9. Bensason D, Simley E, Roberts O, Fleming P, Debnath M, King J, Bay C, Mudafort R. Evaluation of the potential for wake steering for US land-based wind power plants. *J Renew Sustain Energy*. 2021;13(3):033303.
10. Howland MF, Ghate AS, Quesada JB, Pena Martínez JJ, Zhong W, Larrañaga FP, Lele SK, Dabiri JO. Optimal closed-loop wake steering—part 2: diurnal cycle atmospheric boundary layer conditions. *Wind Energy Sci*. 2022;7(1):345-365.
11. Kumar D., Rotea MA, Aju EJ, Jin Y. Wind plant power maximization via extremum seeking yaw control: a wind tunnel experiment. *Wind Energy*. 2023;26(3):247-343.
12. Bernardoni F, Ciri U, Rotea M, Leonardi S. Real-time identification of clusters of turbines. *J Phys: Confer Ser*. 2020;1618:022032.
13. Bernardoni F, Ciri U, Rotea MA, Leonardi S. Identification of turbine clusters during time varying wind direction. In: 2022 American Control Conference (ACC) IEEE; 2022:4236-4241.
14. Wu Y-T, Porté-Agel F. Simulation of turbulent flow inside and above wind farms: model validation and layout effects. *Bound-Layer Meteorol*. 2013;146(2):181-205.
15. Meyer Forsting AR, Troldborg N, Gaunaa M. The flow upstream of a row of aligned wind turbine rotors and its effect on power production. *Wind Energy*. 2017;20(1):63-77.
16. Strickland JMI, Gadde SN, Stevens RJAM. Wind farm blockage in a stable atmospheric boundary layer. Renewable Energy; 2022.
17. Segalini A, Dahlberg J-AA. Blockage effects in wind farms. *Wind Energy*. 2020;23(2):120-128.
18. Segalini A. An analytical model of wind-farm blockage. *J Renew Sustain Energy*. 2021;13(3):033307.
19. Nygaard NG, Steen ST, Poulsen L, Pedersen JG. Modelling cluster wakes and wind farm blockage. *J Phys: Confer Ser*. 2020;1618:062072.
20. Teixeira MAC. The physics of orographic gravity wave drag. *Front Phys*. 2014;2:43.
21. Smith RB. Gravity wave effects on wind farm efficiency. *Wind Energy*. 2010;13(5):449-458.
22. Allaerts D, Meyers J. Boundary-layer development and gravity waves in conventionally neutral wind farms. *J Fluid Mech*. 2017;814:95-130.
23. Allaerts D, Broucke SV, van Lipzig N, Meyers J. Annual impact of wind-farm gravity waves on the Belgian–Dutch offshore wind-farm cluster. *J Phys: Confer Ser*. 2018;1037:072006.
24. Lanzilao L, Meyers J. Set-point optimization in wind farms to mitigate effects of flow blockage induced by atmospheric gravity waves. *Wind Energy Sci*. 2021;6(1):247-271.
25. Lanzilao L, Meyers J. Effects of self-induced gravity waves on finite wind-farm operations using a large-eddy simulation framework. *J Phys: Confer Ser*. 2022;2265:022043.
26. Centurelli G, Vollmer L, Schmidt J, Dörenkämper M, Schröder M, Lukassen LJ, Peinke J. Evaluating global blockage engineering parametrizations with LES. *J Phys: Confer Ser*. 2021;1934:012021.
27. Bleeg J, Purcell M, Ruisi R, Traiger E. Wind farm blockage and the consequences of neglecting its impact on energy production. *Energies*. 2018;11(6):1609.
28. Schneemann J, Theuer F, Rott A, Dörenkämper M, Kühn M. Offshore wind farm global blockage measured with scanning lidar. *Wind Energy Sci Discuss*. 2020;2021:1-26.
29. Debnath M, Scholbrock AK, Zalkind D, Moriarty P, Simley E, Hamilton N, Ivanov C, Arthur RS, Barthelmie R, Bodini N. Design of the American wake experiment (awaken) field campaign. *J Phys: Confer Ser*. 2022;2265:022058.
30. Bernardoni F, Ciri U, Rotea MA, Leonardi S. Identification of wind turbine clusters for effective real time yaw control optimization. *J Renew Sustain Energy*. 2021;13(4):043301.

31. Meyers J, Bottasso C, Dykes K, Fleming P, Gebraad P, Giebel G, Göçmen T, van Wingerden J-W. Wind farm flow control: prospects and challenges. *Wind Energy Sci Discuss*. 2022;2022:1-56.
32. Jonkman J, Butterfiled S, Musial W, Scott G. Definition of a 5-MW reference wind turbine for offshore system development. NREL/TP-500-38060, Golden, Co, USA, NREL - National Renewable Energy Laboratory; 2009.
33. Orlandi P. *Fluid Flow Phenomena: A Numerical Toolkit*: Kluwer Academic; 2000.
34. Orlandi P, Leonardi S. Dns of turbulent channel flows with two- and three-dimensional roughness. *J Turbul*. 2006;7:1-22.
35. Santoni C, Ciri U, Rotea M, Leonardi S. Development of a high fidelity CFD code for wind farm control. In: 2015 American Control Conference (ACC) IEEE; 2015:1715-1720.
36. Santoni C, Carrasquillo K, Arenas-Navarro I, Leonardi S. Effect of tower and nacelle on the flow past a wind turbine. *Wind Energy*. 2017;20(12):1927-1939.
37. Ciri U, Petrolo G, Salvetti MV, Leonardi S. Large-eddy simulations of two in-line turbines in a wind tunnel with different inflow conditions. *Energies*. 2017;10(6):821.
38. Ciri U, Salvetti MV, Carrasquillo K, Santoni C, Iungo GV, Leonardi S. Effects of the subgrid-scale modeling in the large-eddy simulations of wind turbines. *Direct and large-eddy simulation x*: Springer; 2018:109-115.
39. Rocchio B, Ciri U, Salvetti MV, Leonardi S. Appraisal and calibration of the actuator line model for the prediction of turbulent separated wakes. *Wind Energy*. 2020;23(5):1231-1248.
40. Della Posta G, Leonardi S, Bernardini M. A two-way coupling method for the study of aeroelastic effects in large wind turbines. *Renew Energy*. 2022;190:971-992.
41. Johnson KE, Pao LY, Balas MJ, Fingersh LJ. Control of variable-speed wind turbines: standard and adaptive techniques for maximizing energy capture. *IEEE Control Syst Mag*. 2006;26(3):70-81.
42. Laks JH, Pao LY, Wright AD. Control of wind turbines: past, present, and future. In: 2009 American Control Conference (ACC) IEEE; 2009:2096-2103.
43. Orlanski I. A simple boundary condition for unbounded hyperbolic flows. *J Comput Phys*. 1976;21(3):251-269.
44. Santoni C, García-Cartagena EJ, Ciri U, Zhan L, Valerio Iungo G, Leonardi S. One-way mesoscale-microscale coupling for simulating a wind farm in North Texas: assessment against SCADA and LiDAR data. *Wind Energy*. 2020;23(3):691-710.
45. Leonardi S, Castro IP. Channel flow over large cube roughness: a direct numerical simulation study. *J Fluid Mech*. 2010;651:519-539.
46. Sebastiani A, Castellani F, Crasto G, Segalini A. Data analysis and simulation of the Lillgrund wind farm. *Wind Energy*. 2021;24(6):634-648.
47. Jiménez A, Crespo A, Migoya E. Application of a LES technique to characterize the wake deflection of a wind turbine in yaw. *Wind Energy*. 2010;13(6):559-572.
48. Bastankhah M, Porté-Agel F. Experimental and theoretical study of wind turbine wakes in yawed conditions. *J Fluid Mech*. 2016;806:506-541.
49. Nash R, Nouri R, Vasel-Be-Hagh A. Wind turbine wake control strategies: A review and concept proposal. *Energy Convers Manag*. 2021;245:114581.
50. Munters W, Meyers J. Dynamic strategies for yaw and induction control of wind farms based on large-eddy simulation and optimization. *Energies*. 2018;11(1):177.
51. Wen B, Wei S, Wei K, Yang W, Peng Z, Chu F. Power fluctuation and power loss of wind turbines due to wind shear and tower shadow. *Front Mech Eng*. 2017;12(3):321-332.
52. Emeksiz C, Cetin T. In case study: investigation of tower shadow disturbance and wind shear variations effects on energy production, wind speed and power characteristics. *Sustain Energy Technol Assess*. 2019;35:148-159.
53. *Astm international, standard practices for cycle counting in fatigue analysis. technical report e1049-85 (2017)*: ASTM International, West Conshohocken, PA, United States; 2017.
54. Cosack N. Fatigue load monitoring with standard wind turbine signals; 2010.

How to cite this article: Bernardoni F, Rotea MA, Leonardi S. Impact of yaw misalignment on turbine loads in the presence of wind farm blockage. *Wind Energy*. 2024;27(6):535-548. doi:10.1002/we.2899